SANDIA REPORT
SAND2006-2152
Unlimited Release
Printed April 2006

Foam Liquefaction Model under Abnormal Thermal Environment: A Multiphase, Coupled-physics, ALE Approach

Amy C. Sun

Prepared by
Sandia National Laboratories
Albuquerque, New Mexico 87185 and Livermore, California 94550

Sandia is a multiprogram laboratory operated by Sandia Corporation,
a Lockheed Martin Company, for the United States Department of Energy's
National Nuclear Security Administration under Contract DE-AC04-94AL85000.

Issued by Sandia National Laboratories, operated for the United States Department of Energy by Sandia Corporation.

Available to DOE and DOE contractors from
U.S. Department of Energy
Office of Scientific and Technical Information
P.O. Box 62
Oak Ridge, TN 37831

Telephone: (865) 576-8401
Facsimile: (865) 576-5728
E-Mail: reports@adonis.osti.gov
Online ordering: http://www.osti.gov/bridge

Available to the public from
U.S. Department of Commerce
National Technical Information Service
5285 Port Royal Rd.
Springfield, VA 22161

Telephone: (800) 553-6847
Facsimile: (703) 605-6900
E-Mail: orders@ntis.fedworld.gov
Online order: http://www.ntis.gov/help/ordermethods.asp?loc=7-4-0#online

SAND2006-2152
Unlimited Release
Printed April 2006

Foam Liquefaction Model Under Abnormal Thermal Environment: A Multiphase, Coupled-physics, ALE Approach

Amy Sun
Multiphase Transport Processes
Sandia National Laboratories
P.O. Box 5800
Albuquerque, New Mexico 87185-0834

Abstract

Liquefaction has become an important topic to studies of abnormal thermal response of removable epoxy foam (REF). Based on x-ray videos of several component-scale heating experiments, REF undergoes decomposition and a liquefied, mobile phase is visible in all of the tests. Depending on pressure, level of confinement, and orientation of heating, this intermediate phase will either dissolve more foam, flow to other regions, or evaporate quickly. In order to capture the decomposition, liquefaction, and flow characteristics properly, this report describes a multiphase approach to model a foam liquefaction event. The corresponding moving-boundary problem is solved using GOMA. Movement of fluid-solid, vapor-fluid interfaces are tracked based on the arbitrary Lagrangian-Euleran technique. The model was calibrated against a set of side-heated experiments conducted at the Radiant Heat Facility. Results indicate sensitivity with respect to diffusivities of the reacting species and viscosity. The heat load balances in each of the three phases are also analyzed. Currently, this model predicts faster foam recession than experimentally observed due to the adiabatic assumption made about the thermal environment.

Contents

Executive Summary

In this study, the behavior of the liquid phase is included in a computational model for the decomposition of REF under abnormal thermal environment. The motivation stems from experimental observations as well as gaps in our understanding of how liquid impacts the safety theme during a thermal race. Different sets of experiments at the Radiant Heat Facility have yielded evidence of flow [2]. This is especially true when the decomposition products are confined.

Based on understanding deduced from experiments, multi-phase models of two 90^{o}-heated, foam-in-a-can experiments are developed and analyzed as moving boundary problems using GOMA. The first experiment was referred to as the REF8 experiment and the second MFER9 experiment [3]. Each simulation is based on a three-phase model of REF decomposition. Mathematically, the liquid phase is modeled with energy, momentum, and species transport. Only the energy equation is solved for the vapor and solid phases, where thermal transport dominates. The mesh equation is included in all phases. As well as parameters associated with thermal conduction and radiation, the liquid phase requires additional modeling parameters associated with flow, such as viscosity and surface tension. Species transport also requires component-specific parameters, such as diffusivity, mass transfer coefficient and specific volume. The reaction chemistry is based on a two-step kinetics originally developed by Mike Hobbs [6].

Using an arbitrary Lagrangian-Eulerian approach, the finite element mesh for the liquid phase is deformed according to the boundary conditions specified at the solid-liquid and liquid-vapor interfaces [8]. The time-evolution of the interfaces predicted by the simulations is in qualitative agreement with experimental observations. Gravity causes the liquid to displace the vapor in the bottom of the cavity, resulting in asymmetric interfaces. The simulated foam recession rate at steady-state is faster than the observed rate for the REF8 experiment by a factor of four. The discrepancy between experimental and simulated rates is larger for the MFER9 experiment [3]. These differences may be attributed to the assumption of adiabatic surroundings and/or a simple radiation boundary at the vapor-liquid interface.

Case studies with perturbations in several modeling parameters were conducted. By decreasing the gas mass transfer coefficient an order of magnitude to simulate low evaporation, the foam recession rate decreased only slightly. Similar non-sensitivities were observed when lowering viscosity and increasing surface tension. The most sensitivity was observed by decreasing the diffusivities in the liquid phase, which decreased the recession rate significantly. Adding diffusional resistance can be viewed as

decreasing the apparent bulk mixing rate. Perturbations in specific volumes amongst the components did not result in a significant change in overall liquid volume.

As expected, robustness is most impacted by the amount of mesh distortion due to liquid accumulation at the bottom. When evaporation is retarded, more liquid will flow downward, accentuating the asymmetry in the profiles. Other than sensitivity studies, enthalpy information was also analyzed for each phase to understand the impact of thermal load in the liquid phase. The total enthalpy increases as decomposition progresses, with liquid phase accounting for greater than 50% of the energy during the entire process. The conductive, convective, and latent heat fluxes at each phase transition were also analyzed. More work is needed to close the gap between x-ray data and simulations. Nevertheless, valuable information can be extracted from analysis of the multi-phase model.

Figures

Tables

Nomenclature

$\boldsymbol{v}$	velocity vector
$\boldsymbol{v}_m$	mesh displacement velocity
$\boldsymbol{g}$	gravity vector
$\boldsymbol{n}$	normal vector
p	pressure
r_i	rate of the i^{th} reaction
ρ	density
σ	surface tension
σ_B	Boltzman constant
ε	emissivity
μ	viscosity in the liquid phase
k	thermal conductivity
C_p	heat capacity
ΔH_{rxn}	Heat of reaction
T	temperature
T'	dimensionless temperature
T_o	temperature at which demarcation of solid-liquid interface occurs
T_{plate}	heated plate temperature
t	time
F	Foam species
P	Polymer species
$\boldsymbol{J}_i$	Mass flux of the i^{th} species
G_i	Gas species in the i^{th} reaction
k_i	kinetic prefactor for the i^{th} reaction
E_i	Activation energy for the j^{th} reaction
A_i	Arrehnius prefactor in the j^{th} reaction
$\boldsymbol{q}$	heat source contribution from external boundaries
w_i	specific volume of the i^{th} species
y_i	mass fraction of the i^{th} species in the liquid phase
$y_{o,i}$	initial mass fraction of the i^{th} species in the liquid phase
y_i^{vapor}	mass fraction of the i^{th} species in the vapor phase

1. Introduction

Liquefaction of Removable Epoxy Foam (REF) during abnormal thermal decomposition has been observed in past foam-in-a-can tests. While some tests have aided us in gaining understanding of material response under high heat flux, new challenges lie ahead. We derived most of our knowledge from several side-heated (or 90^o-heated) experiments, where visually the flow is most pronounced. The inverted heating orientation results in flowing of REF down the edge of a can, where the x-ray resolution is poorest. Table 1 summarizes all of the 90^o-heated foam-in-can experiments.

Table 1. Summary of the 90^o-heated experiments conducted in 2002 and 2003.

Experiment, date	Heating Orientation	Density, lb/ft^3	Plate Temp, C^o	Formulation	Embedded object	Confine-ment
REF8, 03/02	90^o	8	750	REF200	No	No
MFER9, 06/03	90^o	11	750	REF300	Yes	No
MFER10, 06/03	90^o	11	750	REF300	Yes	No
MFER11, 06/03	90^o	11	900	REF300	Yes	No
MFER12, 06/03	90^o	11	900	REF300	Yes	No
MFER15, 06/03	90^o	11	750	REF300	Yes	No
MFER16, 06/03	90^o	11	750	REF300	Yes	No

Based on the experiments listed in Table 1, some key points from the experiments are worth noting:

- Since the 90^o-heated experiment conducted in March 2002, the formulation for REF has been modified. Hence, the subsequent experiments, referred to as the MFER series, were made with REF200 epoxy. While the change only causes a slight shift in the glass transition temperature, this may have elevated the temperature at which liquefaction takes place. As noted in Table 1, the MFER series were conducted with an embedded component made of stainless steel. Figure 1 shows snapshots of the x-ray images from REF8 and MFER9 experiments. Comparing these images side-by-side, their profiles differ considerably. In both experiments, pyrolysis of foam causes the volume of solid foam to shrink. The decomposition also produces intermediate products that create a flowing medium. Once liquid forms, gravity will induce flow in that region, thus creating different recession speed along the heated surface. The asymmetry between the upper and lower portions of the recession front is less pronounced in the MFER9 experiment than it is in the REF8 experiment. Due to higher foam density and the presence of a stainless steel component, the decomposition front is also slower for MFER. Foam heats up slower around the embedded component than in bulk because the embedded component remains relatively cool throughout MFER experiments.

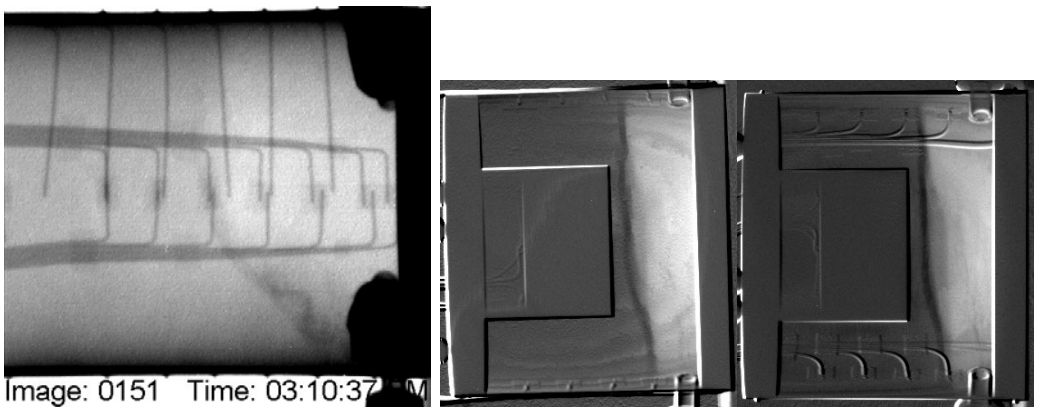

Figure 1. a) Side-heated experiment REF8. t ~3 minutes., T_{top} = 750° C. b) Side-heated experiment MFER9. t ~ 4 minutes, T_{top} = 750 ° C.
(K. Thompson, J. Bentz, K. Erickson, & S. Trujillo)

• We have become increasingly concerned over the residual materials left inside the cans and their possible contribution to the overall heat transfer characteristics. This observation was a possible explanation for a mismatch between experimental data and validation simulations for the thermal model [2]. In the past, the thermal model utilized element-death approach to allow only radiative heat transfer in the enclosure. This new finding challenges the assumption that no attenuation occurs within the burnt cavity.

• REF thermal decomposition under confinement continues to challenge us experimentally and theoretically. Table 2 lists four top-heated foam-in-a-can experiments, two of which were back-pressured and two totally confined. From REF11 and REF20 experiments, we observed increased volumes of intermediate products just by back pressuring the cans. Figure 2a shows a snapshot of REF11 experiment. Figure 2b shows the volumetric fractions of each phase for REF8 and REF11. From x-ray image analysis, the volume of liquid layer in REF11 is comparable to the volume observed in REF8, indicating pressure being another important factor modulating liquefaction. Based on the findings of REF8 and REF11 experiments, two sealed experiments were carried out. HFER experiment was designed specifically to maximize flow effect. In HFER experiment, foam identical to ones used in MFER experiments was hollowed out in the center and heated from the top. Figure 3 shows the schematic and snapshots of HFER experiment. During the experiment, confined decomposed products flowed towards the hollowed region, but the seal was broken after the internal pressure reached 163 psig (15 minutes). The CFER experiment does contain an embedded unit, but it also vented after the experiment reached 600 psig. The behavior of the foam at elevated pressure in total confinement is still difficult to predict.

Table 2. Summary of the confined, high-pressure experiments conducted in 2002 and 2003.

Experiment, date	Heating Orientation	Density, lb/ft^3	Plate Temp, C^o	Formulation	Embedded object	Confine-ment
REF11, 03/02	Top		750	REF100	No	No, 2bar
REF20, 03/02	Top		750	REF100	No	No. 4bar
HFER, 07/03	Top	8	600	REF300	No	<15 min
CFER, 07/03	Top	11	750	REF300	Yes	<30min

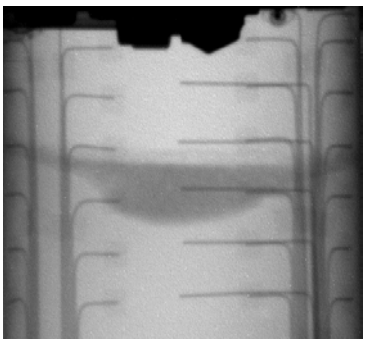

(a)

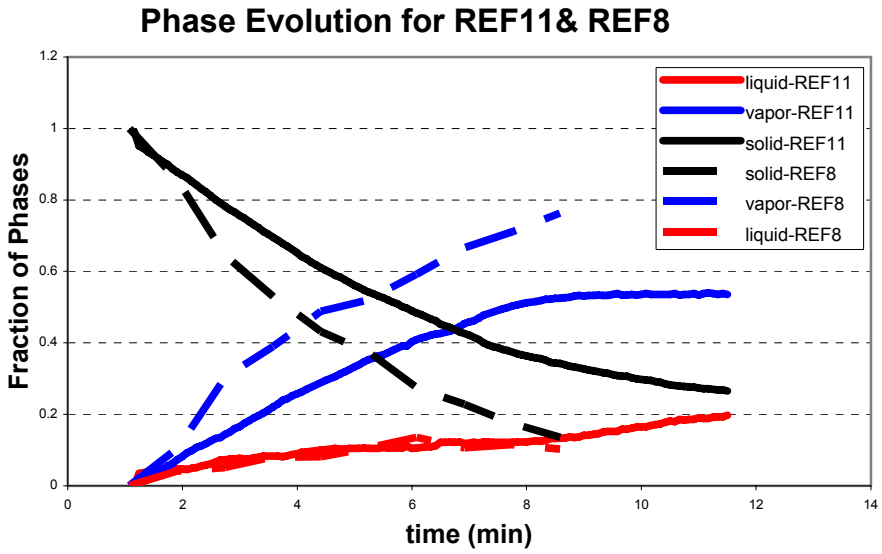

(b)

Figure 2. (a) A snapshot of REF11. (b) Plot of phase fraction as a function of time for REF11 and REF8 experiments. The numbers were compiled from x-ray images.

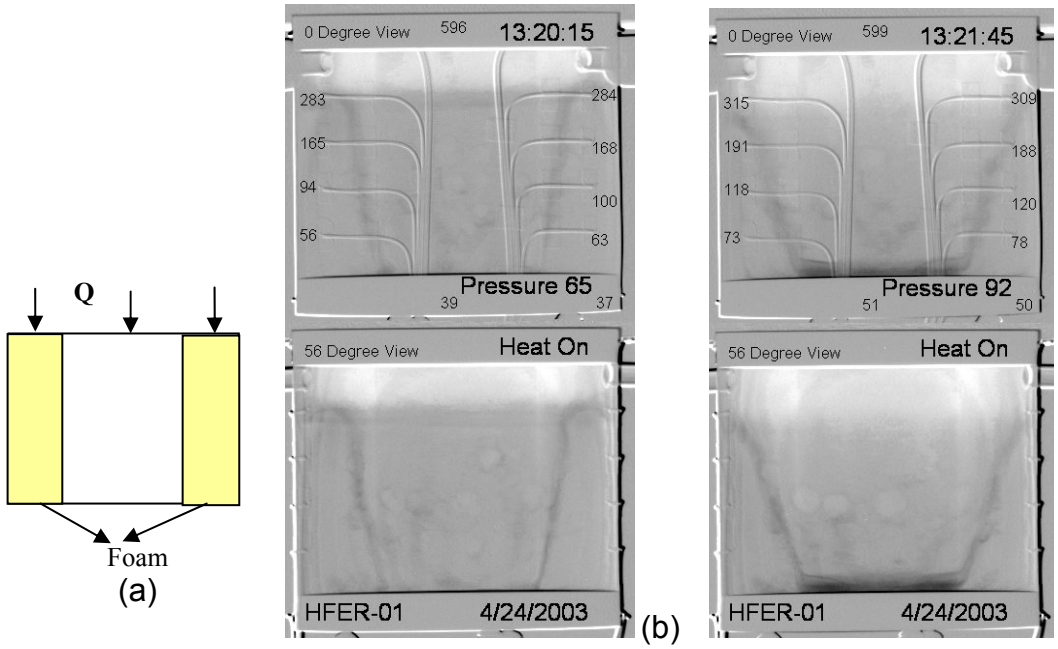

Figure 3. HFER experiment, a) schematic and b) x-ray images (K. Thompson , K. Erickson, & S. Trujillo).

• In order to understand rheological behavior of decomposed foam product at elevated temperatures, we also attempted viscometric measurements of REF. The highest tested, 300^{o}C, in a torsional viscometer yielded little meaningful data as REF deforms under the test unit. Adolf et al. postulated continual bond breakage and formation at 300^{o}C temperature range, with foaming as the primary mode of mobility [1]. The rheological data were however collected in a vented environment. These observations are inconsistent with the evidence that decomposed, liquefied REF drips out of a can in a confined experiment [3].

2. Multiphase Model for REF Thermal Decomposition

To develop a flow model for REF as it undergoes decomposition, modeling phase transitions becomes a necessary component. A multiphase model for 90°-heated geometry was conceptualized and then solved as a moving boundary problem within GOMA [9]. Figure 4 shows a 2D schematic of decomposition dynamics. Due to the high heat flux, the foam pyrolyzes to yield polymeric materials that exhibit flow characteristic before it evaporates into the atmosphere. While demarcations of phase transition are difficult to represent in a model, especially those involving fragmented polymers that evolve dynamically, they must exist as well-defined boundaries in the model. Also note that while the actual FIC geometry is 3D in reality, solving a 2D projection is simpler computationally, and there is much knowledge to be gained by looking at a simpler problem.

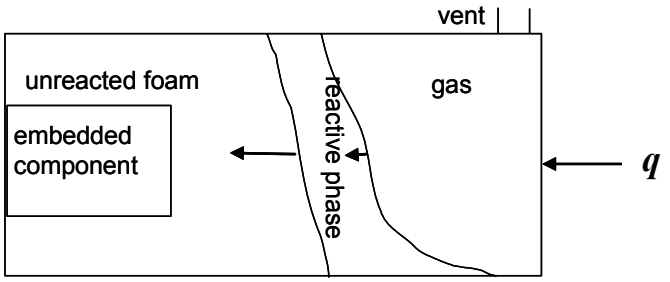

Figure 4. Schematic of 2D model of 90°-heated FIC experiment.

2.1 Bulk Physics

As indicated by Figure 4, the 90°-heated problem contains four computational "domains": gas, reactive phase, unreacted foam, and embedded component. In order to model all four regions using finite element, they must all exist at the start of simulation. Hence, gas and reactive phases are kept at a minimum when they are first meshed. Once geometry has been determined, the physics for each phase is analyzed. Table 3 summarizes the bulk physics for each region.

The first half of Table 3 lists the balance equations for mass, momentum, and energy. The first balance is the momentum equation. The variable v is the fluid velocity, vm mesh velocity, p the pressure, and g the gravitational force. Balance (2) is the continuity equation with a volumetric mass source due to reaction kinetics. The variable ρ_i is pure component density, which is the inverse of specific volume w_i for component i. The variable r_i is the rate expression for reaction i. The decomposition chemistry used for this model, as outlined in balance (3), is crude compared to the recently developed chemistry [4]. Instead of tracking specific chemical species, the reactants and products are pseudo-components in this kinetics. The components are foam (F), product (P), gas (combined G_1 and G_2), and residue (S). Two first-order reactions with Arrhenius-type temperature dependency are used for the kinetics. While more sophisticated reaction mechanisms exist for the REF decomposition, this analysis did not incorporate it. Balance (4) is the

component mass balance, which contains the convective-diffusion portion as well as a reaction source. F, P, G and S are shorthand for foam, product, gas, and residue component respectively. The variable y_i is defined as the mass fraction of either F, P, or G. Mass fraction of S can be deduced by subtracting all independent mass fractions (F, P, and G) from unity, so no component balance for S component is required. The mesh velocity, v_m, is defined as the time derivative of the nodal displacement and solved as a pseudo-elastic solid using pseudo-solid stress balance, balance (5), where $\boldsymbol{T}_s$ is the solid stress. The last balance involves the energy equation, where $\boldsymbol{q}$ is the heat flux vector.

The second half of Table 3 lists the equations used to describe the physics for each phase. GOMA permits different physics to be solved in different domains [9]. The vapor phase does not account for convection of gases or pressurization, so energy balance and mesh equation are solved. Eventually, the effect of pressurization will be added to this model for cases where confinement occurs. This does not preclude the mass transfer resistance in the gas phase, which can be solved as a boundary condition at the liquid/vapor interface. The region of interest, the reactive phase, solves for all of the physics listed in Table 3. Since the reactive phase has mobility due to gravitational force acting on decomposed REF, fluid momentum is specified for that region. Volumetrically, this reactive domain is small; roughly 10% can be inferred by x-ray images of early experiments. Nevertheless, this multi-physics phase makes this model numerically challenging due to combined fluid, mass, and energy transfer. In addition, this phase is compressible due to density changes associated with decomposition. As a result, the problem is inherently stiff with phenomena occurring at different time scales. Like the vapor region, the equations used to solve the behavior of un-reacted foam are energy and mesh balances. As for the embedded component, the heat conduction equation is solved.

Table 3. Summary of bulk physics solved for each region in Figure 3.

Balance	Equations
(1) Momentum	$\rho \frac{d\boldsymbol{v}}{dt} = -\rho(\boldsymbol{v} - \boldsymbol{v}_m) \cdot \nabla \boldsymbol{v} - \nabla p + \nabla \cdot (\mu(\nabla \boldsymbol{v} + \nabla \boldsymbol{v}^T)) + \boldsymbol{g}$
(2) Continuity	$\nabla \cdot \boldsymbol{v} = \sum_i \rho_i r_i, \quad i = F, P, G$ $\rho_i = w_i^{-1}$
(3) Reactions	$F \xrightarrow{k_1} 0.3G_1 + 0.7P$ $P \xrightarrow{k_2} 0.943G_2 + 0.057S$ $r_1 = k_1[F], \quad r_2 = k_2[P], \quad k_j = A_j \exp\left(\frac{-E_j}{RT}\right), \quad j = 1,2$ $G = G_1 + G_2$
(4) Species	$\frac{dy_i}{dt} = (\boldsymbol{v} - \boldsymbol{v}_m) \cdot \nabla y_i - \nabla \cdot \boldsymbol{J}_i + r_i, \quad i = F, P, G$ $y_G = y_{G_1} + y_{G_2}$ $y_S = 1. - y_F - y_P - y_G$
(5) Mesh	$\nabla \cdot T_s = 0$
(6) Energy	$\frac{d(\rho C_p T)}{dt} = (-v_m) \cdot \nabla(\rho C_p T) - \nabla \cdot \boldsymbol{q}$
Vapor Phase	*Energy, Mesh*
Reactive Phase	*Energy, Mesh, Momentum, Continuity, Species, Reaction*
Unreacted Foam	*Energy, Mesh*
Embedded Object	*Energy*

2.2 Interfacial Physics

The shape of the boundaries is tracked by a set of distinguishing conditions. Table 4 summarizes the interfacial physics solved as boundary conditions for this problem.

While the gas-liquid interface is not distinct based on our experimental observations, the model assumes it to be a single boundary. At the vapor-fluid interface, mass transfer of liquid into gas is specified for the species equations. The right hand side describes the mass transfer resistance into the vapor phase. Boundary conditions for the temperature equation consist of radiation and heat of reaction. For the mesh equation, the speed of the mesh at the interface is controlled by the overall mass loss due to evaporation. The velocity at the interface will be satisfied via a surface tension condition, where the fluid stress must be balanced by the surface tension at the interface. The variable $\boldsymbol{T}_{fluid}$ is the fluid stress, P_{ex} the external pressure, H the surface curvature, σ the surface tension, and ∇, the surface divergence operator [7].

The mesh velocity at the solid-fluid interface is driven by an isotherm at 90°C. The term H_{rxn} is the latent heat required for the reactions. It is very important to note that this is <u>not</u> a physical melting boundary but merely a numerical demarcation. The fluid velocity v is set to be zero at the boundary. The boundary conditions for y_o are set to the concentrations of components at 90°C.

Constant temperature is used for the heated plate. The other surroundings are assumed to be adiabatic.

Table 4. Boundary conditions at inter-phases and at the top plate.

Boundary conditions	Equation
Vapor –fluid interphase	Species: $\boldsymbol{n}\cdot\boldsymbol{J}_i+\boldsymbol{n}\cdot(\boldsymbol{v}-\boldsymbol{v}_m)y_i=k_i(y_i-y_i^{vapor}),\quad i=F,P,G.$ Energy: ΔH_{rxn} = 15 cal/gm, $\boldsymbol{n}\cdot\boldsymbol{q}=\varepsilon\sigma_B\left(T^4-T_{plate}^4\right)$ $\varepsilon=0.85,\ \sigma_B=1.355\times10^{-12}\ cal/\sec/cm^2/K^4.$ Mesh: $\boldsymbol{n}\cdot(\boldsymbol{v}-\boldsymbol{v}_m)=\sum_i k_i(y_i-y_i^{gas})$ Momentum: $\boldsymbol{n}\cdot\boldsymbol{T}_{fluid}=-\boldsymbol{n}P_{ex}+2H\sigma\boldsymbol{n}+\nabla_s\cdot\sigma$
Solid-fluid interphase	Energy: ΔH_{rxn} = 45 cal/gm Mesh: $T-T_o=0,\quad T_o=90^0C$ Momentum: $\boldsymbol{v}=0$ Species: $y_i-y_o=0,\quad i=F,P,G$ $y_{o,f}=0.92,\ y_{o,p}=0.055$ and $y_{o,G}=0.024.$
Top plate	Energy: T_{plate} = 750°C. Mesh: $\boldsymbol{v}_m=0$

2.3 Model Parameters

Tables 5 and 6 list the constants used in the simulation. Table 5 lists property constants for the bulk. Vapor phase properties are assumed to be similar to those of air; hence, constants for air are used for that phase. Properties of unreacted foam, between ambient and 90°C, are identical to those used in SREF model [3]. The thermophysical properties for the reactive phase require extrapolation of existing experimental data. Property measurements of REF have been limited to low temperatures, where the polymer structure of the removable epoxy remains relatively unchanged. For example, thermal conductivity of REF without the blowing agent has been measured up to T=195°C. One should expect the extrapolation of physical parameters to high temperatures to exhibit uncertainties, since material properties vary with decomposition. The density for the reactive phase is also estimated based on mass-averaged density of each species in that phase. Lastly, properties for the embedded object are based on reported numbers for SS304 stainless steel.

Table 6 lists the additional parameters necessary for the reactive phase associated with liquid and species transport. Liquid viscosity is a function of temperature. The parameter μ_o is the nominal viscosity value for the foam and E the activation energy for the exponent. Component dependent properties are also required for the reactive phase. Diffusivity, mass transfer coefficient, and specific volume are specified for each component. Note that the units for D, the component diffusivity, is based on a two-dimensional geometry. The reactive phase density is then derived from the inverse of mass-averaged sum of specific volumes, assuming zero volume change due to mixing (note that bulk density is not a weighted average of pure component densities). In addition to component-specific properties, surface tension and specific gravity are required. As discussed in the results section, the surface tension controls the rolling motion of liquefied REF along surfaces and has an impact on the overall convergence of this problem.

All phases are present *a priori* even though presence of reactive and vapor phases evolve later in time. Initially, the reactive and vapor phases each occupy approximately 5% of the total domain. Radiant heat flux is applied with an emissivity of 0.85. The heated surface has a constant temperature of 750°C. The remaining walls of the can are assumed to be adiabatic. Scaling is also applied to the temperature variable to keep its value between 0 and 1; i.e.,

$$T' = \frac{T - T_1}{T_2 - T_1} \quad where\ T_1 = 25^o C\ and\ T_2 = 750^o C$$

Table 5. Bulk phase physical property constants.

Property	Vapor phase	Reactive phase	Unreacted foam	Embedded object
k (cal/cm/sec/K)	6.e-5	5.21e-4	4.42e-4	38.7e-3
Cp (cal/gm/K)	0.240	0.411	0.334	0.120
ρ (gm/cm3)	1.205e-3	see Table 6	0.1296 or 0.1782	8.

Table 6. Additional liquid phase properties.

Property	Value
Viscosity (poise) $\mu(T) = \mu^o \exp(\frac{-E}{RT})$	$\mu_0 = 100.$ E = 0.3 cal/mol
Density (gm/cm3) $\rho = \left(\sum y_i (w_i - w_s) + w_s\right)^{-1}$	$w_G = (0.8\ \rho_f)^{-1}$ $w_F = (\rho_f)^{-1}$ $w_P = (1.2\ \rho_f)^{-1}$
Diffusivity (cm^2/sec)	$D_F = 1.$ $D_G = D_F$ $D_P = D_F$
Mass Transfer Coefficients (1/sec)	$k_G = 10.$ $k_F = 0.$ $k_P = 0.$
Gravity (cm^2/sec)	$g_y = 980.$
Surface tension (mN/m)	$\sigma = 35.$

3. Results

Since this work describes model development work and assessment of liquid flow, comparison between model and experiment has remained qualitative throughout the analysis. Simulation results of REF8 experiment using GOMA are given in Figure 5. The snapshots show foam decomposition at four time points (in seconds). Mesh elements in the vicinity of vapor-liquid interface become distorted, especially near the triple point where liquid, solid wall and gas coincide. The simulation then requires one or two extra remeshing and remapping steps.

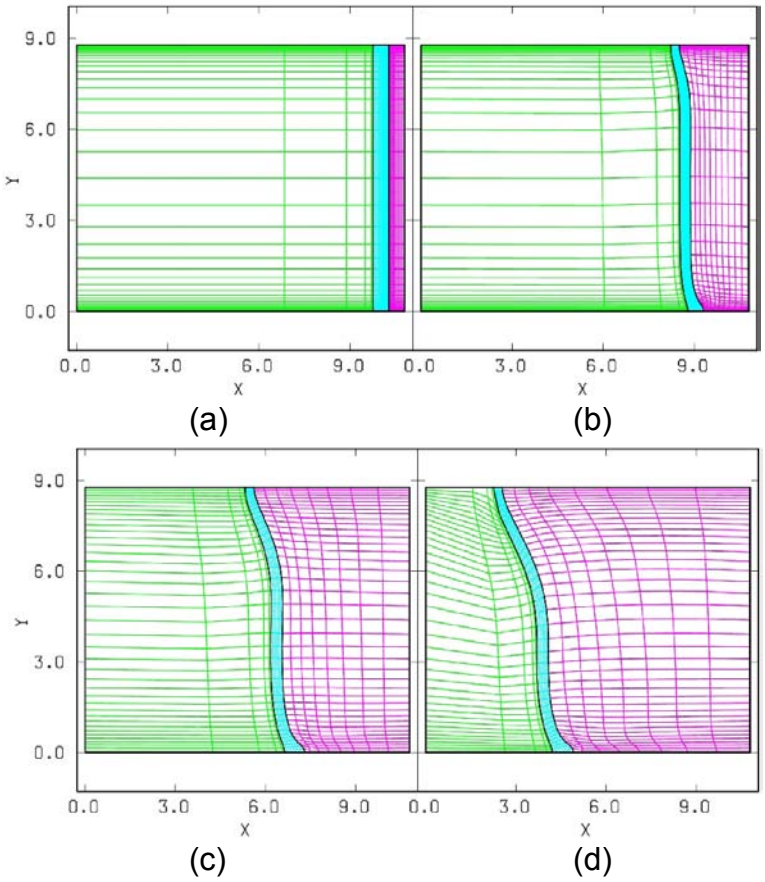

Figure 5. 2D Multiphase foam decomposition, (a) t=0, (b) t=14.8 (c) t=38.5, and t=66 seconds. The unreacted foam, reactive phase and vapor phases are indicated by green, turquoise and pink, respectively. X & y refer to distances in centimeter.

Foam recession is controlled by the heat flux entering the system and modulated by chemistry within the liquid layer. Rate of generation for the reactive material coincides with the movement of T=90^{o}C isotherm. The liquid itself exhibits lower viscosity at higher temperature due to an Arrhenius-type temperature dependency. The shape of liquid meniscus is affected by speed of recession, evaporation of gaseous species, surface

tension, and gravity. Due to gravity-driven flow, the concentration profiles are no longer axi-symmetric (with respect to the centerline). Figures 6a and 6b are plots of temperature and concentration profiles within the reactive phase. The temperature profile across the liquid layer is similar between the upper and lower portions of the 2D domain. Note that "top" and "bottom" designations are referenced against a can on its side, and they are not to be confused with top portion of the can (see schematic in figure 6c). One important assumption made in this model is that the radiation heat flux boundary remains uniform despite flow. As a first approximation, the radiation boundary condition in this model does not vary in the presence of a deformable meniscus to avoid dynamic view factor calculations, but one would expect it to become more inaccurate once the flow is fully developed. The compositions, however, display differences between upper and lower portion of liquid layer. The composition of component P is higher at the bottom of liquid phase than at the top, indicating more decomposition.

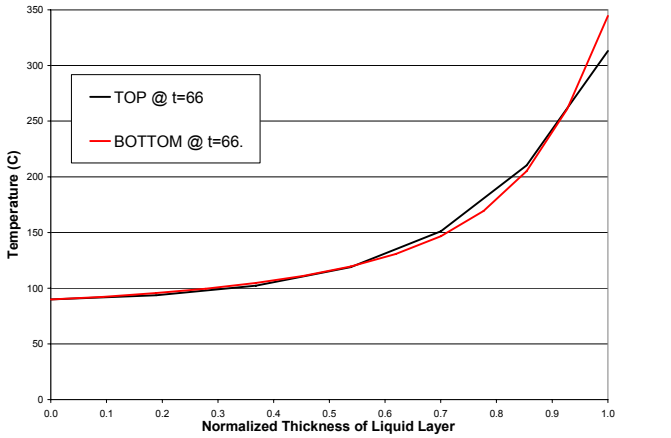

(a)

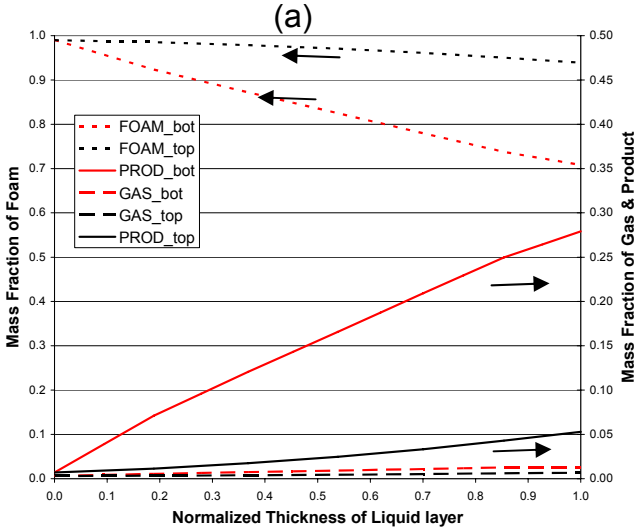

(b)

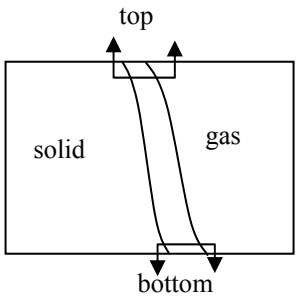

(c)

Figure 6. Temperature and concentration profiles across the liquid phase at upper and lower points along the decomposition front. time =66 seconds. (a) temperature profile (b) concentration profile for foam, product, and gas components (c) schematic.

In Figure 7, MFER9 simulations yielded similar behavior. The simulation proceeds to the point where the solid steel component is almost exposed. The asymmetry is less pronounced in this simulation than in the previous simulation (Fig. 5). The fluid layer is thicker on both sides of the embedded component than the center because the recession is faster around the stainless steel component. This is consistent with the experimental observation. The ALE-based technique can reproduce thinning of the fluid layer, but each interface must remain as one continuous boundary. In reality, this interface will break up around the two solid corners of the embedded object, as indicated in the experiment. Presently, modeling the break-up can be handled by a level-set method.

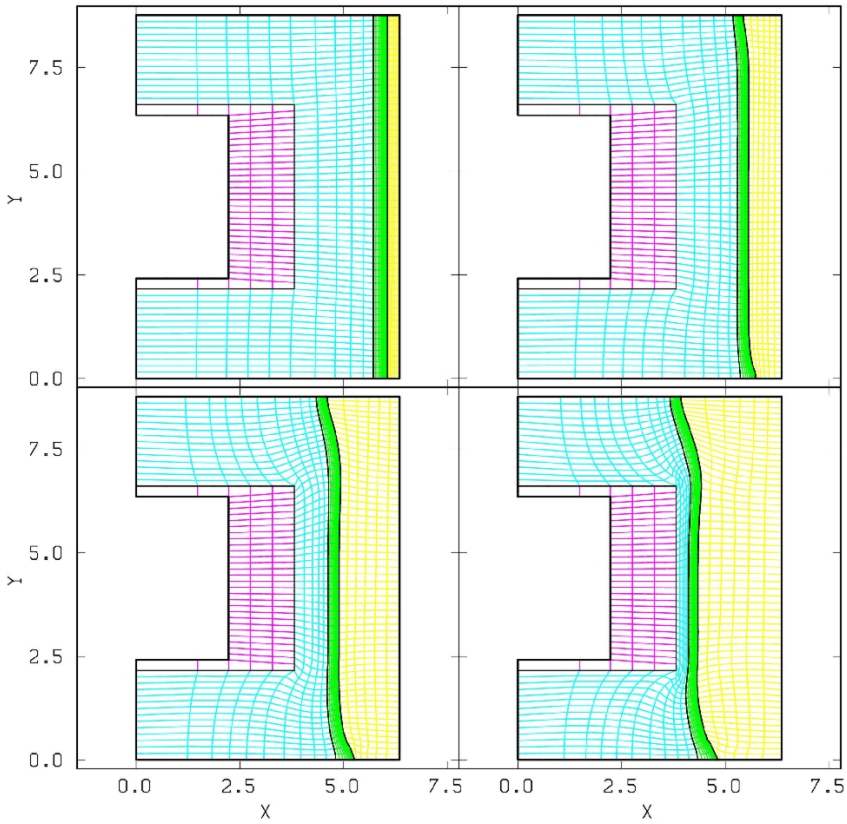

Figure 7. MFER9 simulation. (a) t=0, (b) t=6, (c) t=15, and (d) t=23 seconds. The embedded object, unreacted foam, reactive phase and vapor phases are indicated by pink, turquoise, green and yellow, respectively. X & y refer to distances in centimeter.

In both sets of experiments and simulations, the rate of foam recession is relatively constant after short transient development. The steady-state recession speed of foam in REF8 simulations are 0.11 cm/sec for the top and 0.078 cm/sec for the bottom. These are very fast compared to the ones observed in the experiment (roughly 0.029 cm/sec for the top and 0.012 cm/sec for the bottom), suggesting inaccuracies in the parameters and boundary conditions assumed for the problem. Based on parameters used in simulating REF8 experiment, the steady-state recession speed of foam in MFER9 simulation are 0.091 cm/sec for the top and 0.058 cm/sec for the bottom, as supposed to 0.0077 cm/sec (top) and 0.0047 cm/sec (bottom) observed in the experiment. Larger-than-expected

discrepancy for MFER9 indicates inaccuracies in heat transfer assumptions to the model. By assuming adiabatic walls in the can, it results in higher efficiency of heat transfer to the foam.

The large gap in recession rates can be improved by better descriptions of the incident heat flux at the vapor-liquid interface. As mentioned in the beginning, heat transfer within the vapor phase has become the subject of a concurrent study which will pave the way to better represent a key input quantity in the liquefaction model [6]. In addition, several case studies are presented in the next section to address the sensitivity of model to several parameters.

3.1 Case Studies

Five parameters are perturbed to study the sensitivities of model response. Table 7 summarizes the changes in parameters. Note that the motivation behind this sensitivity analysis is to understand the behavior of fluid phase specifically, so an extensive, blind sensitivity analysis is not warranted at this point. The nominal case is listed first. This is followed by a case in which the mass transfer coefficient of gas component is changed. Another case involves changes in component diffusivities. Perturbations in fluid properties such as surface tension, viscosity, and specific volumes, are also carried out in the next three cases.

The mass transfer coefficient of the gas pseudo-component is first changed to modulate the evaporation rate. An order of magnitude reduction in k_G did not bring an equivalent reduction in the recession speed, indicating other phenomena coupled to the evaporation.

A perturbation in another mass transfer parameter, component diffusivities, was also carried out. Lower diffusivity increases the mass transfer resistance in the bulk phase. A reduction of component diffusivities results in sharper concentration gradients in the reactive phase. Compared to Figure 6, the concentrations plotted in Figure 8 show foam mass fraction to vary from 0.97 to 0 across the fluid layer. The diffusivity can be perceived as an apparent "mixing" constant. From x-ray images, the reactive phase appears as a mobile frothy layer, rather than a pure liquid medium. During decomposition, light-weight volatile components will form bubbles and become immobilized at the solid-liquid interface and "drag" fluid to the vapor-liquid interface. This phenomenon is captured through the diffusion equation. This enhanced mixing is captured by an effective diffusivity. Results of this simulation show streamlines within the liquid phase parallel to the direction of gravity. The diffusivities are set large compared to typical self-diffusivities of common gases or liquids (i.e. $\sim 10^{-2}$ cm^2/sec for gases and $\sim 10^{-5}$ cm^2/sec for liquid). One outcome of increased diffusional resistance is more accumulation of fluid at the bottom of the domain. Figure 9 is a snapshot of the simulation at t = 15 seconds. The asymmetry is greater between the upper and lower sections of liquid domain. The resulting rate is lower for recession of bottom portion of burn front. While both k_G and D_i are difficult to obtain experimentally, they are key parameters to describe the mass transfer phenomenon.

Table 7. Case study matrix (based on REF8 model)

Case Name	σ , (mNm^{-1})	D_i, cm^2/sec	w_i, cm^3/gm	k_G, 1/sec	μ_0 (poise), E (cal/mol)	Recession speed (cm/sec)	Notes
Basecase	35	1	w_P =0.83 w_F, w_G =1.25 w_F	10	100, 0.3	0.11 top 0.085 bottom	x-ray. data (cm/sec) 0.029 top 0.012 bottom
LowEvap	35	1	w_P =0.83 w_F, w_G =1.25 w_F	1.	100, 0.3	0.11 top 0.075 bottom	
LowD	35	0.1	w_P =0.83 w_F, w_G =1.25 w_F	10	100, 0.3	0.11 top 0.047 bottom	
HighSurft	70	1	w_P =0.83 w_F, w_G =1.25 w_F	10	50, 0.3	0.13 top 0.081 bottom	σ_{water} @ 20°C: 70 mNm^{-1} $\sigma_{benzene}$ @ 20°C: 29 mNm^{-1}
LowMu0	35	1	w_P =0.83 w_F, w_G =1.25 w_F	10	50, 0.3	0.13 top 0.078 bottom	μ_{water} @ STP: 0.01 poise $\mu_{glycerol}$ @ 20°C: 10.7 poise
Rho	35	1	w_P =0.67 w_F, w_G =2.0 w_F	10	100, 0.3	0.11 top 0.075 bottom	w_F = 7.71 cm^3/gm

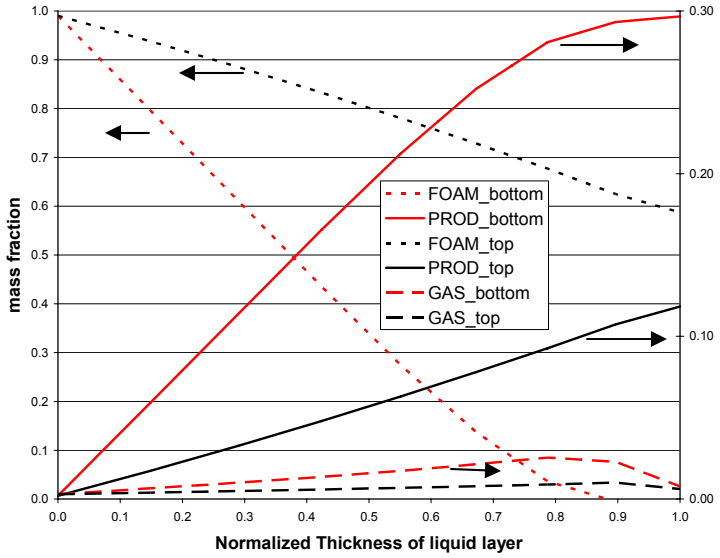

Figure 8. Concentration profiles in LowD case.

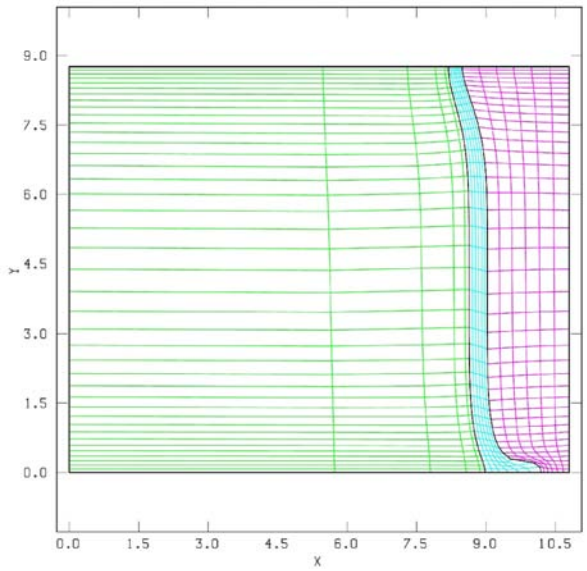

Figure 9. Snapshot of LowD foam recession. t = 15 seconds. X & y refer to distances in centimeter.

The next two case studies involve perturbations in fluid properties. The viscosity influences the bulk flow under gravity, and the surface tension influences the meniscus of interface. The viscosity used for the surface tension study remains identical to the values used in low viscosity case because the surface tension effect is more pronounced at lower bulk viscosity. Figure 10 shows snapshots for these two cases. Similar to the LowD case, greater flow towards the bottom is observed.

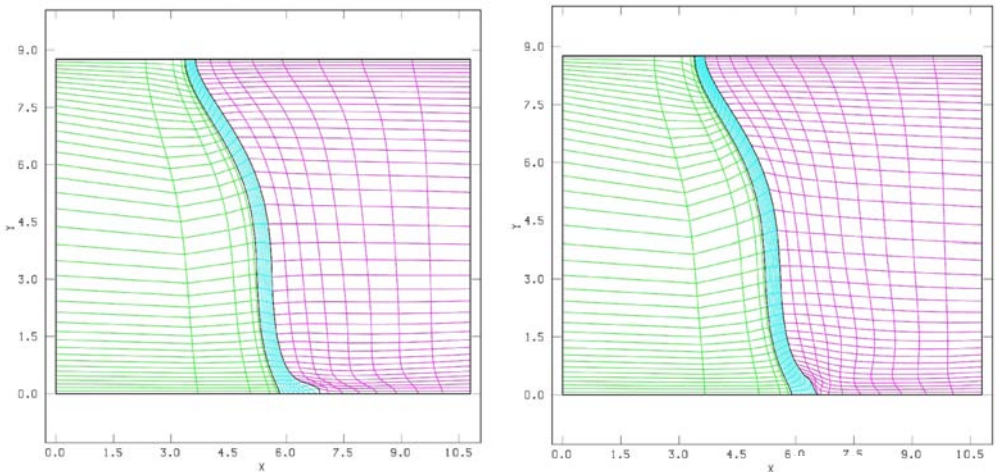

Figure 10. Snapshots of foam recession at t = 50 sec for REF8 simulation. (a) LowMu0 case: more liquid accumulates at the bottom by lowering the viscosity. (b) HighSurft case: the liquid is held more tightly by increasing the surface tension at the vapor-liquid interface. The viscosity parameters are kept the same as in LowMu0 case. X & y refer to distances in centimeter.

The capillary number, a dimensionless group representing relative importance between viscous stress and surface tension, can be calculated based on ranges of constants used in this model.

$$Ca = \frac{\mu U}{\sigma} = \frac{(50 - 100\ poise)\left(\sim 0.1 \frac{cm}{\sec}\right)}{\left(35 - 70 \frac{mN}{m}\right)} = 0.07 - 0.28\ .$$

U is the characteristic velocity for the problem, which is the magnitude of foam recession. The spread of capillary number indicates surface tension more dominant over viscous stress at the vapor-liquid interface.

Another case study is devoted to the sensitivity of model response to a density change (see Table 7). The current specifications have been arbitrarily set for P and G since the reactants and products are pseudo-components. Changes in these quantities did not bring a large change in the recession speed or a significant change in liquid volume. This is due to large concentration of F pseudo-component in the liquid phase (see Figure 6). Even though a large volume difference is imposed between foam and gas species and of foam and product species, concentration of gas is quite low. Hence, the overall volumetric change in the liquid phase is not significant because such low concentrations.

3.2 Enthalpy Analysis

One important goal of developing a multi-physics model and solving the resulting coupled equations is to assess the impact of flow on overall heat transfer. Since each phase domain is created explicitly, the heat load information can be accessed throughout the simulation. It is valuable to analyze the heat load associated with each phase since the contribution from the fluid phase must be assessed to determine its importance. More importantly, this information cannot be obtained based on the current effective thermal conductivity approach [2].

After each time step in each simulation, GOMA calculates the total enthalpy for each phase, the total area for each phase, the heat flux across the solid-liquid and liquid-vapor interfaces, and the gas species flux across the vapor-liquid interface. Table 8 summarizes the equations associated with these post-processing parameters. Because the simulations are based on two-dimensional geometries, the units are in area instead of volume and energy/length instead of energy. In other words, one can assume a semi-infinite volume in all of the simulations conducted for this study.

Table 8. Post-processing quantities.

Enthalpy (cal/cm based on 2D models)	$H = \int \rho C_P (T - T_{ref}) dA$
Area (cm^2)	$A = \int dA$
Heat Flux (cal/sec/cm based on 2D models) solid-liquid & vapor-liquid interfaces	Conductive $\int -k(n \cdot \nabla T) dL$ Convective $\int \rho C_p (T - T_{ref}) \boldsymbol{n} \cdot (\boldsymbol{v} - \boldsymbol{v}_{mesh}) dL$ Latent heat $\int \rho \Delta H_{lat} \boldsymbol{n} \cdot (\boldsymbol{v} - \boldsymbol{v}_{mesh}) dL$
Species Flux (gm/sec/cm based on 2D models) vapor-liquid interface	Diffusive $\int -D_i (n \cdot \nabla y_i) dL$ Convective $\int \rho \boldsymbol{n} \cdot (\boldsymbol{v} - \boldsymbol{v}_{mesh}) y_i dL$ Latent heat $\int \rho \Delta H_{lat} \boldsymbol{n} \cdot (\boldsymbol{v} - \boldsymbol{v}_{mesh}) dL$

Figures 11a and 11b show time evolution of volume and energy of all three phases in the base case. In Figure 11a, the initial transient shows quantity of liquid decreasing when t < 5 seconds. This is due to the assumption that a liquid domain must exist before the start of simulation, and the initial area does not necessarily coincide with the boundary conditions and reactions imposed for that domain. In the subsequent plots of post-processing quantities, the initial transients are ignored. Given that the liquid phase occupies 5% of total area, its total enthalpy is 50% or more of the total energy in the system. This is due to its higher heat capacity and its steep temperature gradient near the VLE phase boundary. Because of the two-dimension models, the units for total enthalpy are energy per length.

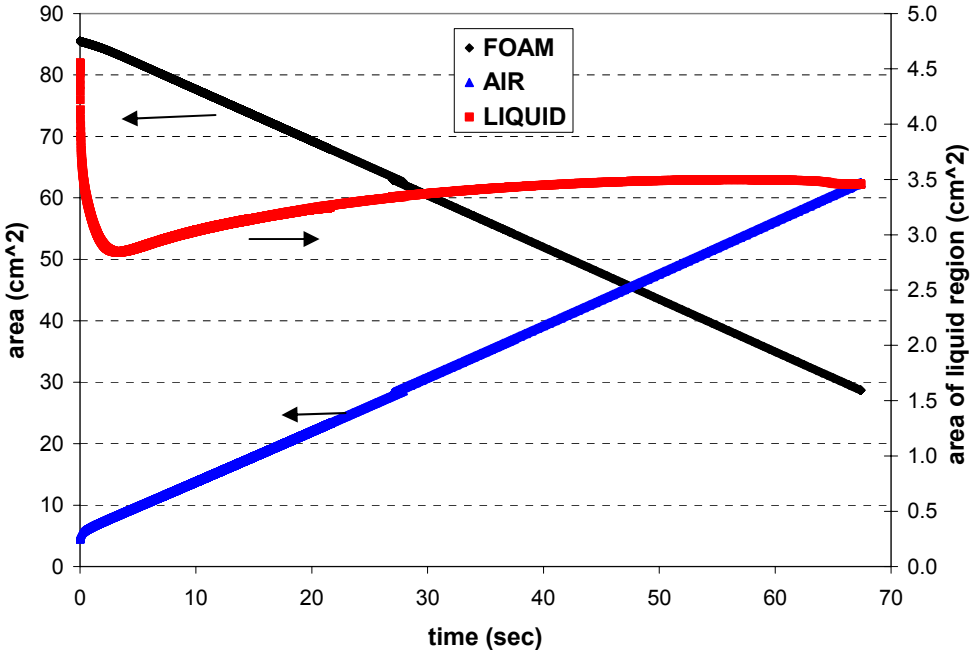

(a)

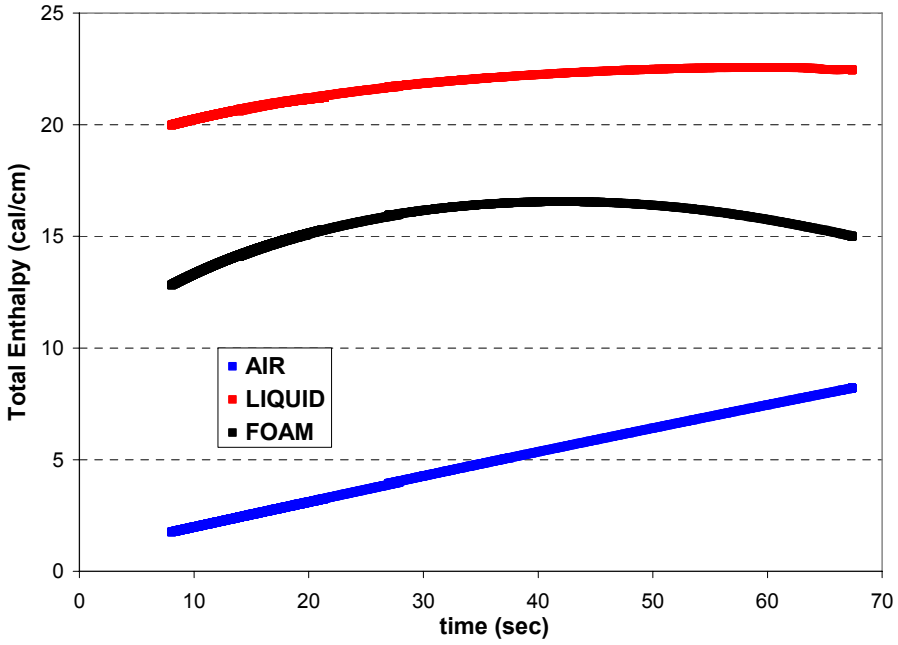

(b)

Figure 11. (a) Area and (b) enthalpy evolution for each phase during simulation of REF8 experiment. The enthalpy unit is based on 2D geometries.

Figure 12a and 12b show plots of heat fluxes across the vapor-liquid (VLE) and liquid-solid (SLE) interfaces. The conductive and convective components have opposite signs, indicating two flow directions (out of domain indicates positive heat flux). Flat curves indicate the heat fluxes reaching steady-state quickly during foam decomposition. Table 9 summarizes the average values.

The convective heat flux is larger in magnitude than the conductive heat flux for each boundary. This is due to the large heat capacity relative to the thermal conductivity for all phases despite small velocity field. Latent heat (or heat of reaction) used for two-step kinetics are applied at the boundaries (rather than in the bulk) and the relative contributions between the two interfacial boundaries are set arbitrarily. Given that the incident flux onto VLE phase boundary is approximately -10. cal/sec/cm (by assuming pure radiation with surface temperature of 315^{o}C), the model is consistent with the approximation.

Table 9. Average heat flux across the interfacial boundary.

	$q_{conductive}$, cal/sec/cm	$q_{convective}$, cal/sec/cm	q_{latent} cal/sec/cm
VLE	-10.	11.	1.38
SLE	-0.33	2.25	4.68

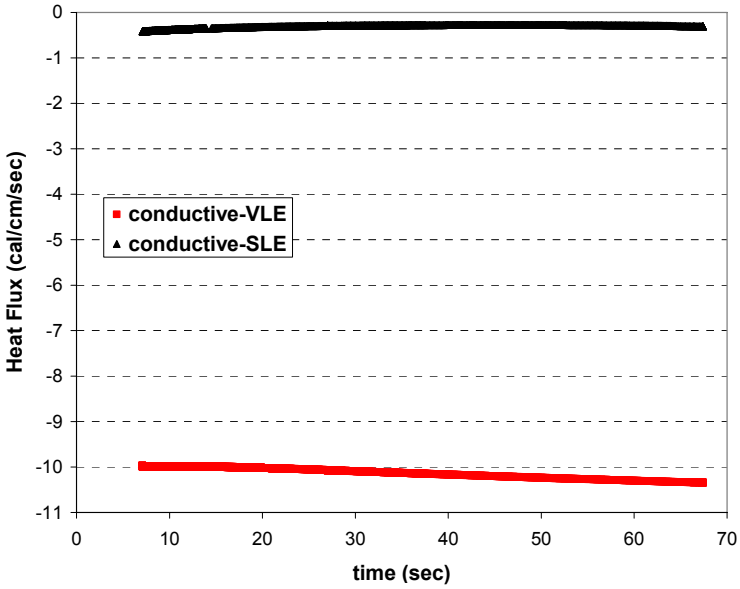

(a)

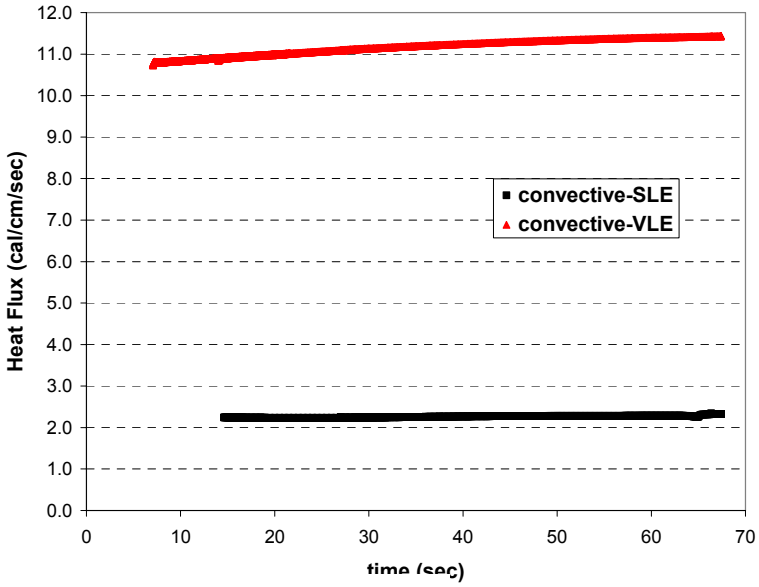

(b)

Figure 12. Distribution of heat fluxes during simulation of REF8 experiment. (a) Conductive heat flux across vapor-liquid and liquid-solid interfaces. (b) Convective heat flux across vapor-liquid and liquid-solid interfaces.

Lastly, figure 13 shows the transient evolution of species flux. The definitions for diffusive and convective fluxes are similar to those defined in Table 8, with thermal conductivity replaced by diffusivity and temperature by mass fraction. The diffusive flux increases with time, but the variation is quite small considering the magnitude of the flux. Changes in diffusive flux are mainly due to changes in gas concentration at the VLE boundary. Verification of mass balance would require data of the outlet gas flow and its corresponding composition, which is not available.

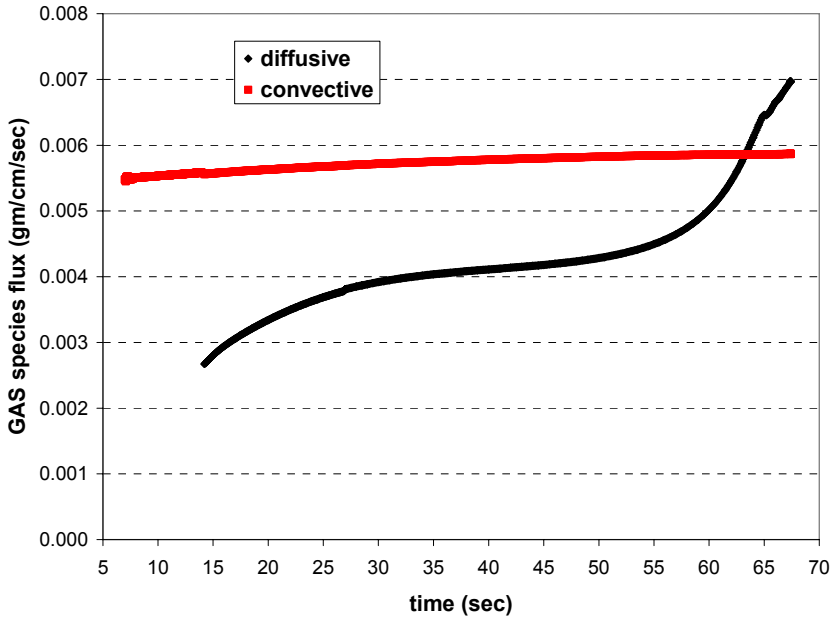

Figure 13. Mass flux across vapor-liquid interface during simulation of REF8 experiment. Specifically, gas species flux is plotted.

4. Conclusion

This memo summarizes the modeling and simulation work for side-heated REF decomposition. This orientation is chosen in order to assess the importance of liquefaction of REF in an abnormal thermal environment. A 2D three-phase model is constructed and solved to simulate REF decomposition as it transitions from an un-reacted solid to a flowing liquid to a gas. The coupled phenomena are simulated within GOMA as a moving boundary problem. The current three-phase model needs improvements in different areas, some of which are discussed in this section.

First, the certainty of liquid phase parameters needs to be improved in order to close the gap between experiment and simulation. Real data for key parameters such as component diffusivities, mass transfer coefficients, viscosities, surface tension, and specific volumes are either scarce or non-existent. Experimental measurements devoted to rheology or dilatometry of decomposed products, or to polymer-air interfacial tension at elevated temperatures will be useful for improving the certainty of model parameters. Together with experimental collaborators, design and manufacturing of a rheometer appropriate for viscosity measurement at high temperatures and high pressures of REF plastic are underway at Georgia Tech. In addition, experiments devoted to visualization of REF flow have been conducted, and its analysis is forthcoming.

Numerically, several challenges lay ahead for coupled-physics modeling of REF decomposition. Solving the entire model in one coupled block can bring unexpected complications on convergence and limits the time step size used for the simulation. Work has only begun to conceptualize a model that can be segregated across domains and/or physics. In conditions where the fluid phase approaches or recedes from sharp corners, the moving mesh approach requires many intermediate re-meshing and remapping steps. Use of level set to track the vapor-liquid interface has also begun to overcome this problem, and its evaluation is forthcoming.

While the current three-phase model is complex, one may still find inadequacy in its current form. For example, the treatment of vapor phase is still crude in the current model. Pressurization and participating media within the vapor phase are two key phenomena yet to be included in this version. Pressurization further influences the partition of decomposed products across vapor-liquid interface. Participating media influences the heat transfer characteristics in the vapor domain. The reactive phase did not consider bubble formation. Visually, generation and collapse of bubbles are observed within that phase and can enhance mixing of liquefied products. The relative importance of these sub-grid level physics to those already in the model is yet to be uncovered.

While the current coupled three-phase model is considered a departure from the effective conductivity model for thermal analysis, it is useful in providing a realistic representation of the entire decomposition process. Without modeling the fluid layer, the sensitivity of key fluid phase properties to the overall heat balance will be lost. In addition, the energy cost associated with the presence of fluid is analyzed in detail in this study. The impact of flow yields an inhomogeneous distribution of material (and therefore heat load). The

effects of orientation become more meaningful when these results are compared to results of current thermal analysis [3,8]. The complementary nature of these two modeling methodologies will enhance the accuracy of REF decomposition model as well as our understanding of foam's impact in a thermal race.

References

1. Adolf, D., S. Kawaguchi, and M. Stavig, "Chemical and Mechanical Characterization of Removable Epoxy Formulation 100," SAND2003-3429.
2. Barra, A.J., B.D. Boughton, K.J. Dowding, V.G. Figueroa, W. Gill, R.E. Hogan, "Validation of calculated W80-3 subsystem mock-up response to abnormal thermal environments, " SAND Report, SAND2004-4749, 2004
3. Erickson, K.L., et al., "Liquefaction and flow behavior of a thermally decomposing removable epoxy foam," Computational Methods in Material Characterisation, pg. 217-242, WIT Press, 2003.
4. Erickson, K.L., et al., "Component-scale Removable Epoxy Foam (REF) Thermal Decomposition Experiments ("MFER" series, April 2003) Supporting the FY04/Q2 Level 1 V&V Milestone. Part 1: Temperature Data." SAND Report in progress.
5. Francis, N.D., "Foam models applied to MVTU-2 exposed to abnormal thermal environments," internal Sandia Memo, 2004.
6. Hobbs, M.L., "SREF – a simple removable epoxy foam decomposition chemistry model," SAND2003-4550.
7. Hobbs, M.L., et al., "Thermal decomposition of polymeric foams: model development based on decomposition chemistry," 4th Tri-lab Engineering Conference on modeling and simulation, October, 2001.
8. Larson, Marvin, "Investigation of an Alternative Effective-k Model for Thermal Transport in Decomposing Foam," in progress.
9. Schunk, P.R., et al., "GOMA 4.0 – A Full-Newton Finite Element Program for Free and Moving Boundary Problems with Coupled Fluid/Solid Momentum, Energy, Mass, and Chemical Species Transport: User's Guide," Sandia Report, SAND2002-3204, 2002.
10. Shelton, J.W. and D. Dobranich, "Calibrating the Foam Decomposition Effective Conductivity Model," internal Sandia Memo, 2004.
11. Sun, A. M.L. Hobbs and K. L. Erickson, "Modeling Multiphase Flow of Liquefied Removable Epoxy Foam", Computational Methods in Material Characterisation, pg. 197-206, WIT Press, 2003.

Distribution:

2	MS9018	Central Technical File	8945-1
2	MS0899	Technical Library	4536
1	MS0833	Dobranich, D.	1516
1	MS0833	Northrop-Salazar, C.	1055
1	MS-0888	Russick, E.M.	1811
1	MS-0824	Chu, T.Y.	1500
1	MS-0824	Hermina, W.	1510
1	MS-0836	Erickson, K.L.	1512
1	MS-0836	Trujillo, S.M.	1512
1	MS-0836	Johannes J.E.	1512
1	MS-0834	Kraynik, A.M.	1514
1	MS-0834	Notz, P.K.	1514
1	MS-0834	Schunk, P.R.	1514
1	MS-0834	Rao, R.R.	1514
1	MS-0834	Mondy, L.A.	1514
1	MS-0836	Gill, W.	1532
1	MS-1135	Hanks, C.R.	1532
1	MS-1135	Belone, B.	1532
1	MS-0828	Dowding, K.J.	1533
1	MS-0828	Hogan Jr., R.E.	1533
1	MS-0836	Barra, A.J.	1516
1	MS-0826	Noble, D.R.	1513
1	MS-0836	Larsen, M.E.	1517
1	MS-0836	Hertel, G.	1516
1	MS-0836	Hobbs, M.	1516
1	MS-0555	Thompson, K.R.	1522

Thomas H. Fletcher
Vince Wilding
Nathan King
Department of Chemical Engineering
Brigham Young University
350 CB, P.O. Box 24100
Provo, UT 84602-4100

Scott Bair
George W. Woodruff School of Mechanical Engineering
Center for High-Pressure Rheology
Atlanta GA 30332-0405